Addendum to "Global constraints on absolute neutrino masses and their ordering"

Francesco Capozzi,[1] Eleonora Di Valentino,[2] Eligio Lisi,[3] Antonio Marrone,[4,3]
Alessandro Melchiorri,[5,6] and Antonio Palazzo[4,3]

[1]*Max-Planck-Institut für Physik (Werner-Heisenberg-Institut), Föhringer Ring 6, 80805 München, Germany*
[2]*Jodrell Bank Center for Astrophysics, School of Physics and Astronomy, University of Manchester, Oxford Road, Manchester M13 9PL, United Kingdom*
[3]*Istituto Nazionale di Fisica Nucleare, Sezione di Bari, Via Orabona 4, 70126 Bari, Italy*
[4]*Dipartimento Interateneo di Fisica "Michelangelo Merlin", Via Amendola 173, 70126 Bari, Italy*
[5]*Dipartimento di Fisica, Università di Roma "La Sapienza", P.le Aldo Moro 2, 00185 Rome, Italy*
[6]*Istituto Nazionale di Fisica Nucleare, Sezione di Roma I, P.le Aldo Moro 2, 00185 Rome, Italy*

(Received 20 March 2020; accepted 5 June 2020; published 22 June 2020)

We revisit our previous work [Capozzi *et al.*, Phys. Rev. D **95**, 096014 (2017)] where neutrino oscillation and nonoscillation data were analyzed in the standard framework with three neutrino families, in order to constrain their absolute masses and to probe their ordering (either normal, NO, or inverted, IO). We include updated oscillation results to discuss best fits and allowed ranges for the two squared mass differences δm^2 and Δm^2, the three mixing angles θ_{12}, θ_{23}, and θ_{13}, as well as constraints on the CP-violating phase δ, plus significant indications in favor of NO vs IO at the level of $\Delta\chi^2 = 10.0$. We then consider nonoscillation data from beta decay, from neutrinoless double beta decay (if neutrinos are Majorana), and from various cosmological input variants (in the data or the model) leading to results dubbed as default, aggressive, and conservative. In the default option, we obtain from nonoscillation data an extra contribution $\Delta\chi^2 \simeq 2.2$ in favor of NO, and an upper bound on the sum of neutrino masses $\Sigma < 0.15$ eV at 2σ; both results—dominated by cosmology—can be strengthened or weakened by using more aggressive or conservative options, respectively. Taking into account such variations, we find that the combination of all (oscillation and nonoscillation) neutrino data favors NO at the level of $3.2 - 3.7\sigma$, and that Σ is constrained at the 2σ level within $\Sigma < 0.12$–0.69 eV. The upper edge of this allowed range corresponds to an effective β-decay neutrino mass $m_\beta \simeq \Sigma/3 \simeq 0.23$ eV, at the sensitivity frontier of the KATRIN experiment.

DOI: 10.1103/PhysRevD.101.116013

I. INTRODUCTION

In a previous work [1] we discussed in detail the constraints on absolute neutrino masses and their ordering arising from a global analysis of world ν data available in 2017, within the standard framework for three neutrino families (3ν). We think it useful to reassess those findings by using more recent experimental results. In particular, we provide updated estimates of mass-mixing oscillation parameters, discuss statistically significant indications in favor of the so-called "normal mass ordering" from (non)oscillation data, and present constraints on absolute ν masses, involving different combinations of cosmological data and models.

This Addendum is structured as follows. In Sec. II we briefly recall the basic 3ν parameters and observables, and the methodology adopted in our analysis. In Sec. III we present updated oscillation data and parameter constraints, including indications in favor of normal ordering. In Sec. IV we discuss recent nonoscillation results from single and double beta decay and from cosmology, with emphasis on the latter—in view of possible departures from "default" choices towards more "aggressive" or "conservative" options, altering the impact on the mass ordering and on absolute ν masses. Taking into account these variants, in the final Sec. V we find upper bounds on the sum of neutrino masses Σ in the range 0.12–0.69 eV at 2σ, and an overall indication for normal ordering at the level of 3.2–3.7σ.

II. PARAMETERS, OBSERVABLES, AND METHODOLOGY

We adopt the standard 3ν framework [2], where the three flavor states ν_α ($\alpha = e, \mu, \tau$) are linear combinations of three massive states ν_i ($i = 1, 2, 3$). The main parameters are the three ν masses m_i, the three mixing angles θ_{ij} and the CP-violating phase δ, supplemented by two extra phases in the case of Majorana neutrinos. Neutrino propagation in matter greatly enriches the phenomenology related to these parameters. See Ref. [3] and references therein.

Concerning neutrino oscillations, their amplitudes and frequencies are sensitive to (at least one) of the angles θ_{ij} and of the squared mass differences Δm^2_{ij}, respectively. We define $\delta m^2 = m_2^2 - m_1^2 > 0$ and $\Delta m^2 = m_3^2 - (m_2^2 + m_1^2)/2$, where $\Delta m^2 > 0$ or < 0 in the so-called normal ordering (NO) or inverted ordering (IO) for the neutrino mass spectrum, respectively. The channel $\nu_\mu \to \nu_e$ provides some sensitivity to δ, as well as to $\pm\Delta m^2$ via matter effects. In the analysis, we start with the minimal dataset sensitive to all the oscillation parameters $(\delta m^2, \pm\Delta m^2, \theta_{ij}, \delta)$, as provided by the combination of solar, KamLAND and long-baseline (LBL) accelerator data. By adding short-baseline (SBL) reactor data, one constrains directly the pair $(\pm\Delta m^2, \theta_{13})$ and, to some extent, the parameters (θ_{23}, δ) via covariances in the fit. Finally, by adding atmospheric data, one further increases the sensitivity to $(\pm\Delta m^2, \theta_{23}, \delta)$. Oscillation data do not constrain absolute ν masses, but reduce the phase space of nonoscillation observables.

Nonoscillation observables include the sum of ν masses Σ probed by cosmology, the effective mass m_β probed in beta decay, and the effective mass $m_{\beta\beta}$ probed in neutrinoless double beta decay (if neutrinos are Majorana); see Refs. [1,3] for definitions. Concerning Σ we remark that, as advocated in Ref. [1], our analysis of cosmological data accounts for three different masses m_i (as dictated by the nonzero values of δm^2 and $\pm\Delta m^2$) and does not assume the degenerate-mass approximation ($m_1 = m_2 = m_3 = \Sigma/3$). Our approach allows one to correctly estimate the NO–IO differences at relatively small values of Σ, and to recover the degenerate case in the limit of high Σ (where NO and IO converge).

Best fits and constraints on the ν parameters are obtained via a χ^2 approach. Single-parameter bounds are obtained by projecting away all the others so that $N_\sigma = \sqrt{\Delta\chi^2}$ defines the distance from the best fit in standard deviation units. This metric can also be applied to test the discrete hypotheses of NO vs IO [3,4]. In the analysis of cosmological data, likelihoods are transformed into effective χ^2 values as described in Ref. [1].

III. OSCILLATION DATA AND CONSTRAINTS

Concerning oscillation data, the analysis presented in Ref. [1] has been updated in a subsequent review [5]. With respect to Ref. [5], we include LBL accelerator data as published by the Tokai-to-Kamioka (T2K) experiment [6] and by the NuMI off-axis ν_e appearance (NOvA) experiment [7]. Concerning SBL reactor data, we include the most recent results from the Daya Bay experiment [8] and the Reactor Experiment for Neutrino Oscillation (RENO) [9]; they dominate the current constraints on θ_{13} and, at the same time, provide a measurement of Δm^2 independent from accelerator and atmospheric data. In the analysis of gallium solar neutrino data (GALLEX-GNO and SAGE) we account for the reevaluation of the ν_e-Ga cross section in Ref. [10], although its effect on the fit turns out to be tiny.

For the sake of completeness, we also mention some recent results that are not included in this work but might be eventually considered in the future: (i) SAGE data with additional exposure have been preliminary reported in Ref. [11], but have not been published yet (to our knowledge); (ii) new Double Chooz measurements of θ_{13} have been released in Ref. [12], but assuming a prior on Δm^2 that prevents inclusion in a global fit; (iii) additional atmospheric ν results have been reported by the Super-Kamiokande (SK) [13] and IceCube Deep Core (IC-DC) [14] experiments, but they have not been cast (yet) in a format that can be reproduced or effectively used outside the collaborations—hence we continue to use the previous χ^2 maps from SK and IC-DC as described in Ref. [5].

The results of our global analysis of oscillation data are reported in Table I, in terms of allowed ranges at 1, 2, and 3σ for each oscillation parameter (the other parameters being marginalized away), for the separate cases of NO and IO. The last column shows the formal 1σ accuracy reached for each parameter. It is interesting to notice that the parameter θ_{23} is now being constrained with an overall fractional accuracy approaching that of θ_{12}, although its best fit remains somewhat unstable, due to the quasidegeneracy of the θ_{23} octants [15]. Also, if one takes the current constraints on δ at face value, then this parameter is already being "measured" with $O(10)\%$ accuracy, around a best-fit value suggestive of nearly maximal CP violation ($\delta \sim 3\pi/2$). However, the CP-conserving value $\delta = \pi$ is still allowed at $\sim 1.6\sigma$ (i.e., at $\sim 90\%$ C.L.) in our global fit, where the CP-violating hint coming from T2K data [6] is somewhat diluted in combination with current NOvA data [7].

Concerning the relative likelihood of IO vs NO, we find that NO is consistently favored in the analysis. Table II shows that the χ^2 difference between the absolute minima increases by enriching the oscillation dataset, up to the value $\Delta\chi^2 = 10.0$ (or 3.2σ) when all data are included. Therefore, if the mass ordering information is also marginalized, only the parameter ranges for NO would survive in Table I.

Figure 1 reports in graphical form the information about the allowed parameter ranges (Table I) and about the IO–NO difference (Table II), including all oscillation data. Our results are consistent with those found in recent global analyses [16,17] and, in particular, are in good agreement with the results in Ref. [17], except for some

TABLE I. Global 3ν analysis of oscillation data, in terms of best-fit values and allowed ranges at $N_\sigma = 1, 2, 3$ for the mass-mixing parameters, in either NO or IO. The last column shows the formal “1σ accuracy” for each parameter, defined as 1/6 of the 3σ range, divided by the best-fit value (in percent). We recall that $\Delta m^2 = m_3^2 - (m_1^2 + m_2^2)/2$ and $\delta/\pi \in [0, 2]$ (cyclic).

Parameter	Ordering	Best fit	1σ range	2σ range	3σ range	“1σ” (%)
$\delta m^2/10^{-5}$ eV^2	NO	7.34	7.20–7.51	7.05–7.69	6.92–7.90	2.2
	IO	7.34	7.20–7.51	7.05–7.69	6.92–7.91	2.2
$\sin^2\theta_{12}/10^{-1}$	NO	3.05	2.92–3.19	2.78–3.32	2.65–3.47	4.5
	IO	3.03	2.90–3.17	2.77–3.31	2.64–3.45	4.5
$\lvert\Delta m^2\rvert/10^{-3}$ eV^2	NO	2.485	2.453–2.514	2.419–2.547	2.389–2.578	1.3
	IO	2.465	2.434–2.495	2.404–2.526	2.374–2.556	1.2
$\sin^2\theta_{13}/10^{-2}$	NO	2.22	2.14–2.28	2.07–2.34	2.01–2.41	3.0
	IO	2.23	2.17–2.30	2.10–2.37	2.03–2.43	3.0
$\sin^2\theta_{23}/10^{-1}$	NO	5.45	4.98–5.65	4.54–5.81	4.36–5.95	4.9
	IO	5.51	5.17–5.67	4.60–5.82	4.39–5.96	4.7
δ/π	NO	1.28	1.10–1.66	0.95–1.90	0–0.07 $\oplus$ 0.81–2	16
	IO	1.52	1.37–1.65	1.23–1.78	1.09–1.90	9

TABLE II. Global 3ν analysis of oscillation data. Difference between the absolute χ^2 minima in IO and NO for increasingly rich datasets, including solar, KamLAND (KL), LBL accelerator, SBL reactor, and atmospheric neutrino data. The latter column reports the same difference in terms of N_σ.

Oscillation dataset	$\Delta\chi^2_{\text{IO–NO}}$	N_σ
LBL acc. + Solar + KL	1.8	1.3
LBL acc. + Solar + KL + SBL reac.	5.1	2.3
LBL acc. + Solar + KL + SBL reac. + Atmos. (=all oscillation data)	10.0	3.2

differences about the relative likelihood of the two θ_{23} octants, that is still “fragile” under small changes in the analysis inputs.

IV. NONOSCILLATION DATA AND CONSTRAINTS

The previous constraints on the oscillation parameters $(\delta m^2, \Delta m^2, \theta_{ij})$ reduce the phase space of the three absolute mass observables $(\Sigma, m_\beta, m_{\beta\beta})$ in both NO and IO [18]. Moreover, as noted, oscillation data disfavor IO at $>3\sigma$. In order to study the sensitivity of nonoscillation data to the mass ordering, it is useful to proceed by including the oscillation constraints on $(\delta m^2, \Delta m^2, \theta_{ij})$ while temporarily ignoring those on the difference $\Delta\chi^2_{\text{IO–NO}}$, taken as null instead of $\Delta\chi^2_{\text{IO–NO}} = 10.0$. The latter value will be reintroduced, after completing the nonoscillation data analysis, in the global data combination.

Figure 2 shows the allowed regions for $(\Sigma, m_\beta, m_{\beta\beta})$ as derived from oscillation data only, in terms of 2σ and 3σ bands. The high accuracy achieved in measuring the oscillation parameters is reflected by the small difference between the 2 and 3σ contours, as well as by the small width of the bands in the plane charted by the pair (Σ, m_β), not affected by unknown Majorana phases as $m_{\beta\beta}$. In this figure we take $\Delta\chi^2_{\text{IO–NO}} = 0$, as discussed above; if the value 10.0 were used, the IO bands would disappear.

Let us now discuss the update of nonoscillation data. Concerning $m_{\beta\beta}$, a compilation of recent results from neutrinoless double beta decay ($0\nu\beta\beta$) searches has been reported and discussed in Ref. [19]. In particular, Table I therein shows the 90% C.L. upper limits on $m_{\beta\beta}$ from single experiments (in terms of their sensitivity for null signal with $m_{\beta\beta} = 0$ at best fit), as well as a combined limit $m_{\beta\beta} <$ 66–155 meV at 90% C.L., where the numerical range reflects the spread of nuclear matrix elements in the literature, see Ref. [19]. For the sake of simplicity we adopt their median limit, $m_{\beta\beta} < 110$ meV at 90% C.L., corresponding to assume $m_{\beta\beta} = 0 \pm 0.07$ eV (1σ error) as $0\nu\beta\beta$-decay input datum in our χ^2 analysis. We note that the corresponding upper limit at 2σ, $m_{\beta\beta} < 0.14$ eV, is slightly stronger than the analogous limit $m_{\beta\beta} < 0.18$ eV in our previous analysis [1], and reflects the incremental progress in this field.

Concerning m_β, the KATRIN Collaboration recently reported their first and very promising results, which can be summarized as $m_\beta^2 = -1.0^{+0.9}_{-1.1}$ eV^2 at 1σ [20]. By symmetrizing the lower error (unimportant in our parameter space) to match the upper one, we take $m_\beta^2 = -1.0 \pm 0.9$ eV^2 as β-decay input datum in the χ^2 analysis. A more refined approach using the full likelihood profile for m_β^2 [20] is not necessary for the purposes of this Addendum, since the impact of m_β on neutrino masses is still weak as compared with that of $0\nu\beta\beta$ or Σ (although it will become relevant with future KATRIN data). In general, as we shall see below, the sensitivity of nonoscillation data to neutrino

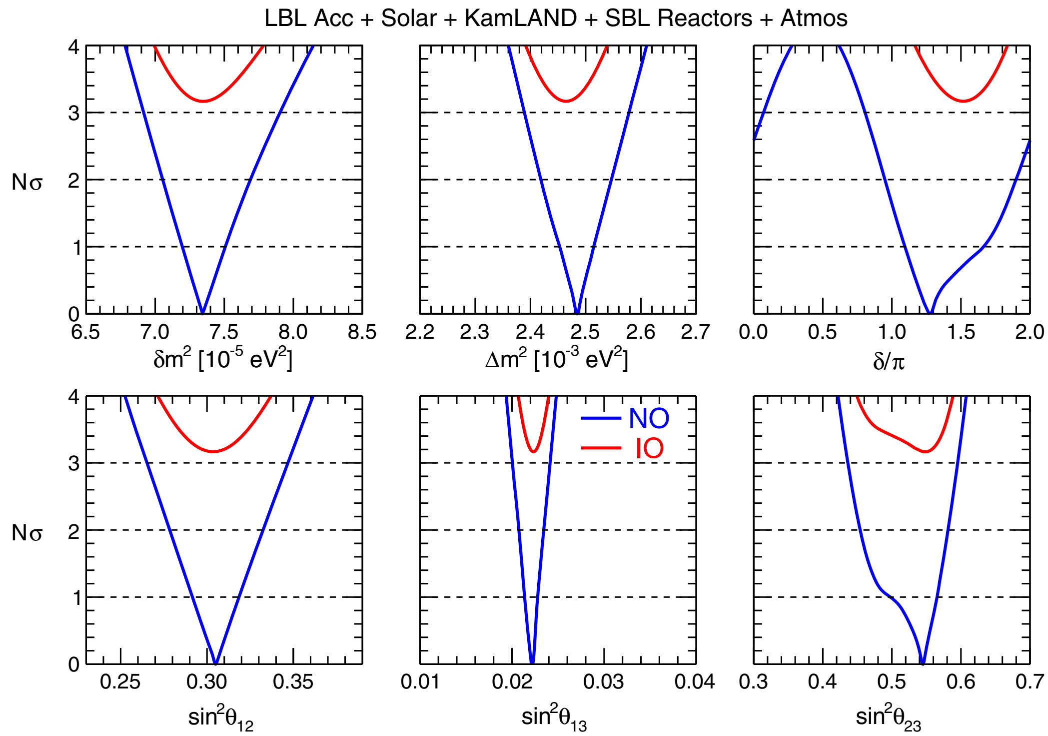

FIG. 1. Global 3ν oscillation analysis. Bounds on the parameters δm^2, $|\Delta m^2|$, $\sin^2\theta_{ij}$, and δ, for NO (blue) and IO (red), in terms of $N_\sigma = \sqrt{\Delta\chi^2}$ from the best fit. In each panel we account for the overall offset $\Delta\chi^2_{\text{IO-NO}} = 10.0$, disfavoring the IO case by 3.2σ.

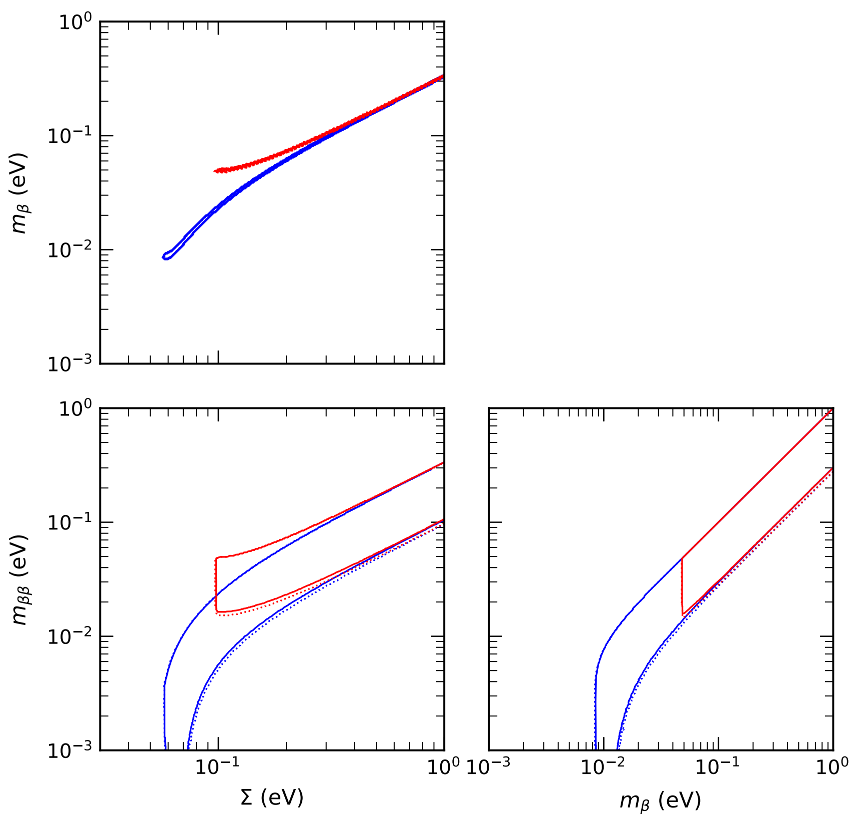

FIG. 2. Oscillation bounds on the nonoscillation observables $(\Sigma, m_\beta, m_{\beta\beta})$, in each of the three planes charted by a pair of such observables. Bounds are shown as contours at 2σ (solid) and 3σ (dotted) for NO (blue) and IO (red) taken separately. Majorana phases are marginalized away. Note that we take $\Delta\chi^2_{\text{IO-NO}} = 0$ in this figure.

masses and their ordering is dominated by the cosmological constraints on Σ and associated variants, so that very refined approaches to both m_β and $m_{\beta\beta}$ constraints do not really matter (yet).

As in Ref. [1], we consider a default cosmological model and dataset(s) plus some variants, in order to present constraints ranging from aggressive to conservative ones. Our default model is the so-called ΛCDM cosmology augmented with ν masses ($\Lambda\text{CDM} + \Sigma$), that depends on the following basic parameters: the baryon and the cold dark matter densities ω_b and ω_{cdm}, the amplitude and tilt of primordial scalar fluctuations A_s and n_s, the reionization optical depth τ, and the angular size of the acoustic horizon at decoupling θ_{MC} (see Refs. [21–24] for recent reviews). Our default dataset includes, in progression, the following experimental inputs:

(i) The Planck measurements of cosmic microwave background (CMB) anisotropies from the final 2018 legacy release adopting the same methodology used by the Planck Collaboration. We, therefore, consider a combination of different likelihoods, using the `commander` likelihood for large scale ($\ell < 30$) temperature anisotropies, the `SimAll` likelihood for large scale polarization anisotropies, and the `Plik` likelihood for temperature, polarization, and cross temperature-polarization anisotropies at small angular scales ($30 \leq \ell \leq 2500$). This is the baseline hybrid likelihood used by the Planck Collaboration (see Refs. [25,26]). In what follows we refer to this dataset as Planck TT, TE, EE. With respect to the Planck 2015 release used in Ref. [1], the new data are now more reliable in the case of the polarization power spectra, with a significant improvement on large angular scales. We, therefore, do not consider anymore the case of Planck temperature alone as in our previous paper [1].

(ii) The new measurements of the CMB lensing potential power spectrum over multipoles $8 \leq L \leq 400$, also derived from the final Planck 2018 data release [27]. We refer to this dataset as "lensing."

(iii) A compilation of baryon acoustic oscillation (BAO) measurements, given by data from the 6dFGS [28], SDSS MGS [29], and BOSS DR12 [30] surveys. We refer to this dataset as "BAO."

It should be noted that alternative datasets might provide constraints comparable to our default ones. In particular, the Lyα-forest data from Ref. [31] would produce, in combination with Planck measurements, a 2σ bound $\Sigma < 0.14$ eV [31]. As already noted in Ref. [25], this bound is close to the one obtained from the Planck+BAO+lensing analysis that, in our case, gives $\Sigma < 0.15$ eV (see below). In this sense, our default choice of data manages to cover well the typical constraints on ν masses, as derived from current experimental results within the $\Lambda\text{CDM} + \Sigma$ model. In addition, we have altered the previous default choice, by enlarging either the dataset or the model (with different outcomes on neutrino mass constraints), in order to account for some emerging tensions with Planck 2018 data.

In particular, as additional "discrepant" data we consider a prior on the Hubble constant as measured by the SH0ES Collaboration [32] (Riess *et al.* 2019, dubbed `R19`), analyzing type-Ia supernovae data from the Hubble Space Telescope using 70 long-period Cepheids in the Large Magellanic Cloud as calibrators. This prior is $H_0 = 74.03 \pm 1.42$ km/s/Mpc at 1σ and we refer to it as $H_0(\mathtt{R19})$. The tension of this prior with Planck 2018 data leads, as we shall see, to tighter constraints on the neutrino mass. We have considered also an alternative prior on H_0 derived from the revised measurement of the Large Magellanic Cloud Tip of the Red Giant Branch extinction from Ref. [33] (Freedman *et al.* 2020, dubbed `F20`), namely, $H_0(\mathtt{F20}) = 69.6 \pm 1.9$ km/s/Mpc, where the quoted statistical and systematics errors have been added in quadrature. We have verified that the combination Planck + R19 covers the range of neutrino constraints that are obtained by the alternative combinations Planck + F20. Therefore, we shall present results for $H_0(\mathtt{R19})$ only, as a paradigmatic example of additional data leading to aggressive neutrino bounds.

Conversely, some data tensions may be formally relaxed by adding extra degrees of freedom to the model. In particular, the amount of gravitational lensing in the Planck 2018 CMB spectra is larger than what is expected in the ΛCDM scenario by nearly 3 standard deviations [25]. As in Ref. [1], we, therefore extend the $\Lambda\text{CDM} + \Sigma$ model via an additional parameter A_{lens} parameter, that simply rescales the lensing amplitude in the CMB spectra, in order to minimize the effect of this anomaly on the cosmological bounds on the neutrino mass. We refer to this extended scenario as $\Lambda\text{CDM} + \Sigma + A_{\mathrm{lens}}$. While the constraints obtained in this case on Σ are weaker and, therefore, more conservative, it is important to note that the A_{lens} parameter is unphysical and that may not properly describe the physical nature of the anomaly. However, it illustrates a possible conservative scenario for neutrino mass constraints.

In all cases (default, aggressive, and conservative), the cosmological constraints on Σ are obtained using the `CosmoMC` code [34], based on a Monte Carlo Markov chain algorithm. Probability posteriors on Σ are obtained after marginalization over the remaining nuisance parameters.

In Table III we organize the information about cosmological models, input data, and fit results as follows. The first row includes the "0th" case with Planck TT, TE, EE data alone. The following three rows include our default options 1–3, where Planck data are combined with either lensing or BAO inputs or both. In the rows numbered as 4–6, with respect to the cases 1–3 we include the Hubble parameter prior $H_0(\mathtt{R19})$, which leads to more aggressive constraints on neutrinos, at the price of introducing some tension in the fit. Finally, in the rows numbered as 7–9, with

TABLE III. Results of the 3ν analysis of cosmological data. Our default scenario is based on the standard ΛCDM + Σ model and on Planck 2018 angular CMB temperature power spectrum (TT) plus polarization power spectra (TE, EE), with the addition of data from the lensing potential power spectrum (lensing) and BAO, separately or in combination (cases No. 1–3). A more aggressive scenario is obtained by adding the Hubble constant datum from HST observations of Cepheids in the Large Magellanic Cloud measurements, H_0(R19) (cases No. 4–6). Conversely, a more conservative scenario is obtained by adding an extra degree of freedom (A_{lens}) to the model (cases No. 7–9). For each case we report the 2σ upper bound on the sum of ν masses Σ (marginalized over NO and IO), together with the $\Delta\chi^2$ difference between IO and NO, using cosmology only. In the last two columns, we report the same information as in the previous two columns, but adding m_β and $m_{\beta\beta}$ constraints, inducing minor variations. For simplicity, in the text we refer to the cases numbered 3, 6, and 9 as representative of default, aggressive, and conservative options, respectively.

Cosmological inputs for nonoscillation data analysis			Results: Cosmo only		Cosmo + m_β + $m_{\beta\beta}$	
No.	Model	Dataset	$\Sigma(2\sigma)$	$\Delta\chi^2_{\mathrm{IO-NO}}$	$\Sigma(2\sigma)$	$\Delta\chi^2_{\mathrm{IO-NO}}$
0	ΛCDM + Σ	Planck TT, TE, EE	<0.34 eV	0.9	<0.32 eV	1.0
1	ΛCDM + Σ	Planck TT, TE, EE + lensing	<0.30 eV	0.8	<0.28 eV	0.9
2	ΛCDM + Σ	Planck TT, TE, EE + BAO	<0.17 eV	1.6	<0.17 eV	1.7
3	ΛCDM + Σ	Planck TT, TE, EE + BAO + lensing	<0.15 eV	2.0	<0.15 eV	2.2
4	ΛCDM + Σ	Planck TT, TE, EE + lensing + H_0(R19)	<0.13 eV	3.9	<0.13 eV	4.0
5	ΛCDM + Σ	Planck TT, TE, EE + BAO + H_0(R19)	<0.13 eV	3.1	<0.13 eV	3.2
6	ΛCDM + Σ	Planck TT, TE, EE + BAO + lensing + H_0(R19)	<0.12 eV	3.7	<0.12 eV	3.8
7	ΛCDM + Σ + A_{lens}	Planck TT, TE, EE + lensing	<0.77 eV	0.1	<0.69 eV	0.1
8	ΛCDM + Σ + A_{lens}	Planck TT, TE, EE + BAO	<0.31 eV	0.2	<0.30 eV	0.3
9	ΛCDM + Σ + A_{lens}	Planck TT, TE, EE + BAO + lensing	<0.31 eV	0.1	<0.30 eV	0.2

respect to the cases 1–3 we allow an extra degree of freedom A_{lens} that tends to relax the fit, leading to more conservative results. In the Table, the fourth and fifth columns show the results of the cosmological data analysis, in terms of 2σ upper bounds on Σ (marginalized over NO and IO) and $\Delta\chi^2$ difference between IO and NO. As expected, aggressive or conservative options lead to stronger or weaker indications with respect to the default ones. [We have also replaced the prior H_0(R19) with H_0(F20) (not shown), obtaining less aggressive results, closer to the default ones.] In any case, with respect to our 2017 analysis [1], all bounds on Σ are now within the sub-eV range, and the overall indication in favor of NO is more pronounced. These indications remain basically unchanged, or are just slightly corroborated, by including subdominant constraints from β and $0\nu\beta\beta$ data, as shown in the last two columns.

In the following two figures, we provide further information complementary to that in Table III. For the sake of graphical clarity, in each group of three cases (1–3, 4–6, and 7–9) we select only the most complete ones (3, 6, and 9) as representative of default, aggressive, and conservative options, respectively.

Figure 3 shows the $\Delta\chi^2$ curves for NO and IO (using cosmological data only), with respect to the absolute χ^2 minimum, that is reached in NO in all cases. One can notice that, in each of the three representative options, the curves tend to converge for increasing values of Σ as they should, up to residual differences (not larger than $\delta\chi^2 \simeq 0.1$ at any Σ), which quantify the small numerical uncertainty of the analysis. The curves would converge also at small Σ in the degenerate approximation $m_1 + m_2 + m_3$, that we discard since we do include the oscillation constraints on δm^2 and Δm^2 in the cosmological fit. As a result, we can correctly quantify the χ^2 differences arising between IO and NO at

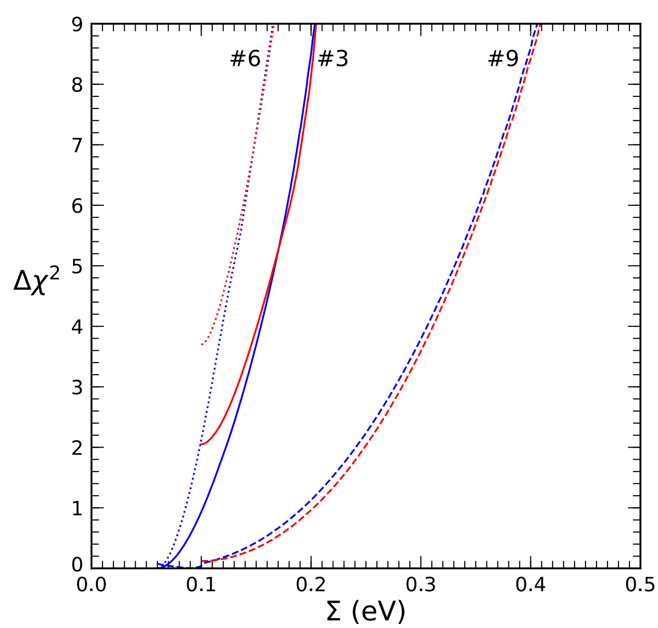

FIG. 3. $\Delta\chi^2$ curves for NO (blue) and IO (red) from the analysis of cosmological data, corresponding to cases numbered in Table III as 6 (left, dotted), 3 (middle, solid) and 9 (right, dashed). These cases are representative of aggressive, default, and conservative options, respectively. Note that, in any case, upper bounds on Σ can be placed in the sub-eV range, and that IO is generally disfavored (although only by a tiny amount in the conservative case 9).

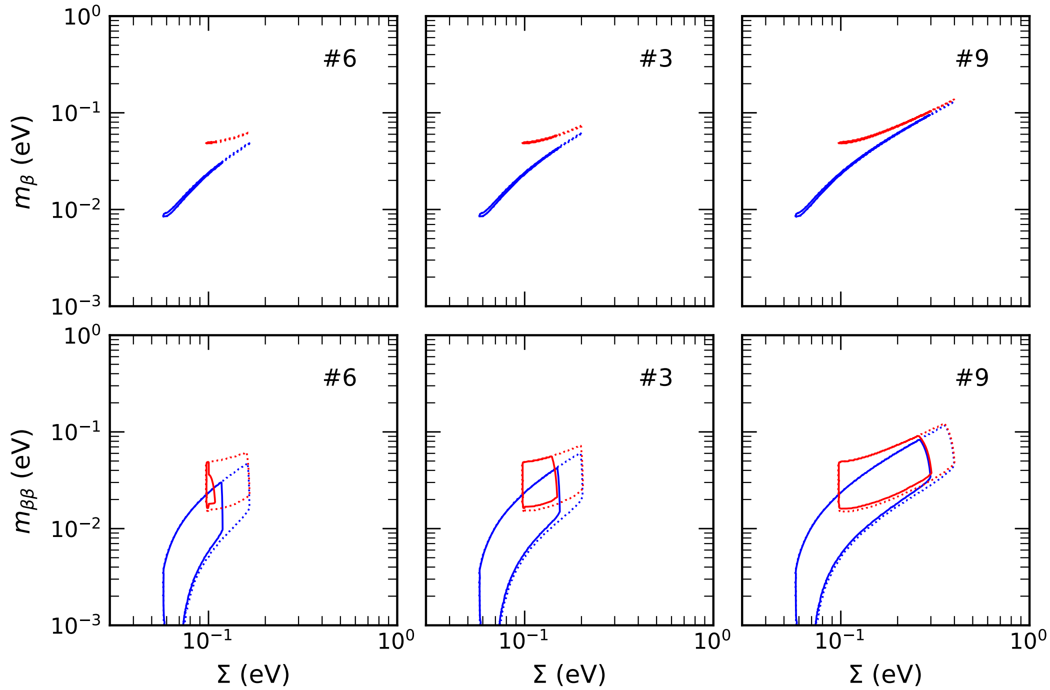

FIG. 4. Bounds at 2σ (solid) and 3σ (dotted) for NO (blue) and IO (red), as derived by including nonoscillation data with respect to Fig. 2, in the upper and lower panels charted by (Σ, m_β) and by $(\Sigma, m_{\beta\beta})$, respectively. The bounds include the $\Delta\chi^2$ difference between IO and NO, as reported in the last column of Table III. The pairs of panels on the left, in the middle, and on the right correspond to the cases No. 6, No. 3, and No. 9 in Table III, respectively.

small values of Σ, as shown in this figure and numerically reported in the fifth column of Table III.

Figure 4 shows how the constraints in the planes $(\Sigma, m_{\beta\beta})$ and (Σ, m_β) are modified (with respect to those in Fig. 2) by the fit to nonoscillation data from cosmology, single and double beta decay. The left, middle, and right panels correspond to the cases numbered in Table III as 6 (aggressive), 3 (default), and 9 (conservative), respectively. Allowed regions are always present in IO, since nonoscillation data do not yet discriminate IO from NO at $> 2\sigma$ in any of the cases that we have considered. Of course, the IO regions would disappear by adding also the indications in favor of NO derived from oscillation data.

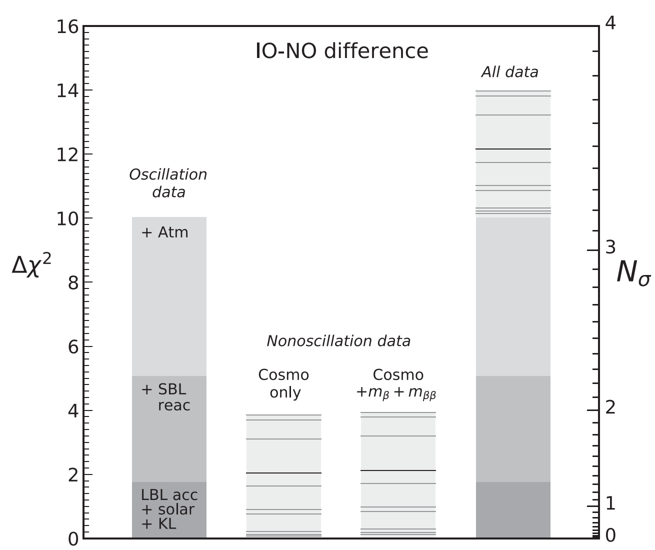

FIG. 5. Breakdown of contributions to the IO–NO difference from oscillation and nonoscillation data. The latter span a range of cosmological input variants (default, aggressive, and conservative). See the text for details.

When a direct comparison is possible, our cosmological constraints agree well with the results from similar analyses [35–37]. A Bayesian combination of such constraints with those from $0\nu\beta\beta$ decay has been considered in Ref. [38], where the upper bound $m_{\beta\beta} < 0.031$ eV was obtained for $\Sigma < 0.14$ eV (at 2σ for NO). Our closest case in No. 3 in Fig. 4, where we obtain $m_{\beta\beta} < 0.04$ eV for $\Sigma < 0.15$ eV; the results are in the same ballpark, with secondary differences due to alternative statistical approaches.

V. SYNTHESIS AND CONCLUSIONS

We conclude this Addendum by merging the information coming from oscillation and nonoscillation data. This merging does not alter the bounds on the sum of neutrino masses Σ already reported in the sixth column of Table III, and that can be summarized as follows:

$$\Sigma < 0.15 \text{ eV (default)}, \tag{1}$$

$$\Sigma < 0.12\text{–}0.69 \text{ eV (range)}, \tag{2}$$

where we have singled out our default case No. 3, and reported the whole range spanned by cases No. 0–9, covering variants more conservative or aggressive than the default one. The upper edge of this range corresponds to an effective β-decay neutrino mass $m_\beta \simeq \Sigma/3 \simeq 0.23$ eV, at the sensitivity frontier of the KATRIN experiment [20].

Concerning the mass ordering discrimination, merging oscillation and nonoscillation data enhance the indications in favor of NO, since the $\Delta\chi^2$ contributions in the second columns of Table II and in the last column of Table III add coherently. The overall indication in favor of NO can be summarized as follows, in standard deviation units:

$$N_\sigma(\text{IO–NO}) = 3.5 \ (\text{default}), \tag{3}$$

$$N_\sigma(\text{IO–NO}) = 3.2 - 3.7 \ (\text{range}). \tag{4}$$

Figure 5 shows the separate and global contributions to the $\Delta\chi^2(\text{IO–NO})$ difference in graphical form (histogram). The first bin represents a breakdown of the contributions from oscillation data, as derived in Table II. The second bin shows the range spanned by all the cases considered in Table III, for the fit to cosmological data only. Each case corresponds to a horizontal line, with the tick one marking our default case No. 3. The third bin shows the slight change induced by adding m_β and $m_{\beta\beta}$ constraints, as reported in the last column of Table III. Finally, the fourth bin, obtained by summing the first and third bins, provides the overall indications on mass ordering from oscillation and nonoscillation data. The vertical axis on the right side translates the results in terms of N_σ. Although none of the single oscillation or nonoscillation datasets provides compelling evidence for normal ordering yet, their current combination is impressively in favor of this option.

In conclusion, building upon our previous work [1], we have presented improved constraints on absolute neutrino masses and indications on their ordering (favored to be normal), as well as updated bounds on the neutrino oscillation parameters (including hints on the *CP* phase). In this context, the interplay of oscillation and nonoscillation data remains an important tool to reach a consistent picture of neutrino masses and mixings.

ACKNOWLEDGMENTS

This work is partly supported by the Italian Ministero dell'Università e Ricerca (MUR) through the research Grant No. 2017W4HA7S "NAT-NET: Neutrino and Astroparticle Theory Network" under the program PRIN, and by the Istituto Nazionale di Fisica Nucleare (INFN) through the "Theoretical Astroparticle Physics" (TAsP) project. The work of F. C. is supported by the Deutsche Forschungsgemeinschaft through Grant No. SFB-1258 "Neutrinos and Dark Matter in Astro- and Particle Physics (NDM)" and EXC 2094 "ORIGINS: From the Origin of the Universe to the First Building Blocks of Life". The work of E. D. V. is supported by the European Research Council through Consolidator Grant No. 681431. Preliminary results of this work have been presented in various conferences.

[1] F. Capozzi, E. Di Valentino, E. Lisi, A. Marrone, A. Melchiorri, and A. Palazzo, Global constraints on absolute neutrino masses and their ordering, Phys. Rev. D **95**, 096014 (2017).
[2] M. Tanabashi *et al.* (Particle Data Group), Review of particle physics, Phys. Rev. D **98**, 030001 (2018), and 2019 update.
[3] M. C. Gonzalez-Garcia and M. Yokoyama, Review on "Neutrino Masses, Mixing and Oscillations" in [2].
[4] Y. Uchida, M. Hartz, R. P. Litchfield, C. Wilkinson, and A. Kaboth, PhyStat-ν 2016 at the IPMU: Summary of discussions, arXiv:1806.10913.
[5] F. Capozzi, E. Lisi, A. Marrone, and A. Palazzo, Current unknowns in the three neutrino framework, Prog. Part. Nucl. Phys. **102**, 48 (2018).
[6] K. Abe *et al.* (T2K Collaboration), Constraint on the matter-antimatter symmetry-violating phase in neutrino oscillations, arXiv:1910.03887.
[7] M. A. Acero *et al.* (NOvA Collaboration), First Measurement of Neutrino Oscillation Parameters using Neutrinos and Antineutrinos by NOvA, Phys. Rev. Lett. **123**, 151803 (2019).
[8] D. Adey *et al.* (Daya Bay Collaboration), Measurement of the Electron Antineutrino Oscillation with 1958 Days of Operation at Daya Bay, Phys. Rev. Lett. **121**, 241805 (2018).
[9] G. Bak *et al.* (RENO Collaboration), Measurement of Reactor Antineutrino Oscillation Amplitude and Frequency at RENO, Phys. Rev. Lett. **121**, 201801 (2018).
[10] J. Kostensalo, J. Suhonen, C. Giunti, and P. C. Srivastava, The gallium anomaly revisited, Phys. Lett. B **795**, 542 (2019).
[11] V. Gavrin, The history, present and future of SAGE (Soviet-American Gallium Experiment), in *Proceedings of the 5th International Solar Neutrino Conference (Dresden, Germany, 2018)*, edited by M. Meyer and K. Zuber (World Scientific, Singapore, 2019), p. 588.
[12] H. de Kerret *et al.* (Double Chooz Collaboration), First double Chooz θ_{13} measurement via total neutron capture detection, arXiv:1901.09445.

[13] M. Jiang *et al.* (Super-Kamiokande Collaboration), Atmospheric neutrino oscillation analysis with improved event reconstruction in Super-Kamiokande IV, Prog. Theor. Exp. Phys. **2019**, 053F01 (2019).
[14] M. G. Aartsen *et al.* (IceCube Collaboration), Development of an analysis to probe the neutrino mass ordering with atmospheric neutrinos using three years of IceCube DeepCore data, Eur. Phys. J. C **80**, 9 (2020).
[15] G. L. Fogli and E. Lisi, Tests of three flavor mixing in long baseline neutrino oscillation experiments, Phys. Rev. D **54**, 3667 (1996).
[16] P. F. de Salas, D. V. Forero, C. A. Ternes, M. Tortola, and J. W. F. Valle, Status of neutrino oscillations 2018: 3σ hint for normal mass ordering and improved *CP* sensitivity, Phys. Lett. B **782**, 633 (2018).
[17] I. Esteban, M. C. Gonzalez-Garcia, A. Hernandez-Cabezudo, M. Maltoni, and T. Schwetz, Global analysis of three-flavour neutrino oscillations: Synergies and tensions in the determination of θ_{23}, δ_{CP}, and the mass ordering, J. High Energy Phys. 01 (2019) 106, Updated results: NuFIT 4.1 (2019), www.nu-fit.org.
[18] G. L. Fogli, E. Lisi, A. Marrone, A. Melchiorri, A. Palazzo, P. Serra, and J. Silk, Observables sensitive to absolute neutrino masses: Constraints and correlations from world neutrino data, Phys. Rev. D **70**, 113003 (2004).
[19] M. Agostini *et al.* (GERDA Collaboration), Probing Majorana neutrinos with double-β decay, Science **365**, 1445 (2019).
[20] M. Aker *et al.* (KATRIN Collaboration), Improved Upper Limit on the Neutrino Mass from a Direct Kinematic Method by KATRIN, Phys. Rev. Lett. **123**, 221802 (2019).
[21] K. H. Olive and J. A. Peacock, Review on "Big-Bang Cosmology" in [2].
[22] O. Lahav and A. R. Liddle, Review on "Cosmological Parameters" in [2].
[23] J. Lesgourgues and L. Verde, Review on "Neutrinos in Cosmology" in [2].
[24] D. Scott and G. F. Smoot, Review on "Cosmic Microwave Background" in [2].
[25] N. Aghanim *et al.* (Planck Collaboration), Planck 2018 results. VI. Cosmological parameters, arXiv:1807.06209.
[26] N. Aghanim *et al.* (Planck Collaboration), Planck 2018 results. V. CMB power spectra and likelihoods, arXiv:1907.12875.
[27] N. Aghanim *et al.* (Planck Collaboration), Planck 2018 results. VIII. Gravitational lensing, arXiv:1807.06210.
[28] F. Beutler, C. Blake, M. Colless, D. H. Jones, L. Staveley-Smith, L. Campbell, Q. Parker, W. Saunders, and F. Watson, The 6dF Galaxy survey: Baryon acoustic oscillations and the local Hubble constant, Mon. Not. R. Astron. Soc. **416**, 3017 (2011).
[29] A. J. Ross, L. Samushia, C. Howlett, W. J. Percival, A. Burden, and M. Manera, The clustering of the SDSS DR7 main Galaxy sample I. A 4 per cent distance measure at $z = 0.15$, Mon. Not. R. Astron. Soc. **449**, 835 (2015).
[30] S. Alam *et al.* (BOSS Collaboration), The clustering of galaxies in the completed SDSS-III Baryon Oscillation Spectroscopic Survey: Cosmological analysis of the DR12 galaxy sample, Mon. Not. R. Astron. Soc. **470**, 2617 (2017).
[31] C. Yèche, N. Palanque-Delabrouille, J. Baur, and H. du Mas des Bourboux, Constraints on neutrino masses from Lyman-alpha forest power spectrum with BOSS and XQ-100, J. Cosmol. Astropart. Phys. 06 (**2017**) 047.
[32] A. G. Riess, S. Casertano, W. Yuan, L. M. Macri, and D. Scolnic, Large magellanic cloud Cepheid Standards provide a 1% foundation for the determination of the Hubble constant and stronger evidence for physics beyond ΛCDM, Astrophys. J. **876**, 85 (2019).
[33] W. L. Freedman *et al.*, Calibration of the Tip of the Red Giant Branch (TRGB), arXiv:2002.01550.
[34] A. Lewis and S. Bridle, Cosmological parameters from CMB and other data: A Monte Carlo approach, Phys. Rev. D **66**, 103511 (2002).
[35] S. Roy Choudhury and S. Hannestad, Updated results on neutrino mass and mass hierarchy from cosmology with Planck 2018 likelihoods, arXiv:1907.12598.
[36] M. Lattanzi and M. Gerbino, Status of neutrino properties and future prospects–Cosmological and astrophysical constraints, Front. Phys. **5**, 70 (2018).
[37] S. Gariazzo, M. Archidiacono, P. F. de Salas, O. Mena, C. A. Ternes, and M. Tortola, Neutrino masses and their ordering: Global data, priors and models, J. Cosmol. Astropart. Phys. 03 (2018) 011.
[38] S. Dell'Oro, S. Marcocci, and F. Vissani, Empirical inference on the Majorana mass of the ordinary neutrinos, Phys. Rev. D **100**, 073003 (2019).